

# Comparative Microstructural Study of Cold Sprayed Coatings Using Pure Aluminum and Aluminum Alloy Powders <sup>†</sup>

Jiashuo Qi <sup>1</sup>, Rija Nirina Raelison <sup>2,\*</sup> , Christophe Verdy <sup>2</sup>, Jishuai Li <sup>1,3</sup> and Mohamed Rachik <sup>1</sup>

<sup>1</sup> Laboratoire Roberval, Université de Technologie de Compiègne, Alliance Sorbonne Université, Centre de Recherche Royallieu, CS 60319, 60203 Compiègne, France; jiashuo.qi@utc.fr (J.Q.); jishuai.li@outlook.com (J.L.); mohamed.rachik@utc.fr (M.R.)

<sup>2</sup> Laboratoire Interdisciplinaire Carnot de Bourgogne (ICB), Université de Technologie de Belfort-Montbéliard, CNRS, 21078 Dijon, France; christophe.verdy@utbm.fr

<sup>3</sup> Institute of Mechanics, Materials and Civil Engineering, Université Catholique de Louvain, 1348 Louvain-la-Neuve, Belgium

\* Correspondence: rija-nirina.raoelison@utbm.fr

<sup>†</sup> Presented at the 15th International Aluminium Conference, Québec, QC, Canada, 11–13 October 2023.

**Abstract:** Cold gas dynamic spraying is a solid-state processing technique that is particularly attractive for surface coatings, 3D near-net shape additive manufacturing, and component repairs with an advantage of high-deposition efficiency. This technique has the sustainable potential to change the future industrial and manufacturing environment, especially in the fabrication process of complex flight-critical components that are made of aluminum. This paper investigates the microstructure of aluminum coatings generated onto a commercial Al plate called FORTAL (Al 7075-T6) via cold spraying using helium as the propellant gas. Three Al coatings (pure Al, AlSi10Mg, and Scalmalloy) are compared under a similar deposition condition. The top view of the coating revealed the highest deformation (high flattening) in the case of pure Al powders, whereas both the AlSi10Mg and Scalmalloy powders exhibit less flattening. The cross sections show fine equiaxed grains within the pure Al coating and extremely fine grains for both the AlSi10Mg coating and the Scalmalloy coating, with more extremely refined grains within the Scalmalloy coating. These results suggested an onset of recrystallization within the Al coating that is attributed to the heat generated by the strong plastic deformation. Less thermally activated recrystallization occurred within both AlSi10Mg coating and Scalmalloy coating due to their stronger mechanical properties. The structure rather resulted from the dynamic due to the high strain rate collision. The extremely fine structure is mostly at the powder/powder interface within the Scalmalloy coating and is developed towards the powder region which is also within the AlSi10Mg coating. Better plastic deformation occurred within the AlSi10Mg powder compared to the Scalmalloy powder that have a higher mechanical resistance. Together, these results evidence a limited thermally activated recrystallization within the Al alloys despite the highest deposition condition being used. The pure Al powders can also achieve a state of equiaxed fine grain due to the better plastic deformation.

**Keywords:** cold spray; coating; microstructure; aluminum alloys



**Citation:** Qi, J.; Raelison, R.N.; Verdy, C.; Li, J.; Rachik, M. Comparative Microstructural Study of Cold Sprayed Coatings Using Pure Aluminum and Aluminum Alloy Powders. *Eng. Proc.* **2023**, *43*, 7. <https://doi.org/10.3390/engproc2023043007>

Academic Editor: Houshang Alamdari

Published: 12 September 2023



**Copyright:** © 2023 by the authors. Licensee MDPI, Basel, Switzerland. This article is an open access article distributed under the terms and conditions of the Creative Commons Attribution (CC BY) license (<https://creativecommons.org/licenses/by/4.0/>).

## 1. Introduction

Cold gas dynamic spray (CGDS) is an emerging solid-state powder deposition additive manufacturing technology, which is widely used in the repair of various parts and the near-net shape of high-performance large components [1]. Unlike various high-energy beam additive manufacturing technologies, metallic materials do not need to undergo melting and solidification during the cold spraying deposition process [2–4]. Therefore, the powder particles of metal materials are not easy to be oxidized during the deposition process [5]. Cold spray technology has significant advantages for depositing heat-sensitive and oxidizable materials. Aluminum and its alloys have gained great attention in both

industrial and academic areas due to their outstanding properties such as low density, high ductility, good corrosion resistance, and excellent thermal and electrical conductivity. In cold gas dynamic spray additive manufacturing, aluminum and its alloys are preferred over other kind of metal materials due to their high deposition efficiency and lower melting point [6]. Effective regulation of performance, especially the key mechanical properties, is the prerequisite for promoting the wide application of cold spray technology. For a given aluminum material that can undergo very strong plastic deformation, its microstructure is the key to determining whether its target properties can be achieved [7].

In this paper, we report the comparative microstructural features of cold sprayed (CSed) Al 1050, AlSi10Mg, and Scalmalloy, respectively. In our study, the microstructural evolution of the Al 1050, AlSi10Mg, and Scalmalloy coatings from the feedstock powders to the deposit as a result of the high strain rate self-consolidation is evaluated by means of scanning electron microscopes (SEM) equipped with electron backscatter diffraction (EBSD). In order to gain insight into the bonding mechanism between the coatings and the particles and between particles, the microstructure at the appropriated locations is selected for analysis.

## 2. Materials and Methods

We have characterized particle flight behavior in terms of the process parameters including gas inlet conditions, powder properties, and nozzle dimensions in previous studies [8–11]. In this study, the commercially atomized powders of Al 1050, AlSi10Mg, and Scalmalloy from Toyal are used as spraying powders. An Al 7075 T6 plate is used as a substrate. Three plates are printed with three aluminum powders using He. Before the sprayed process commences, these three substrates are sandblasted in order to obtain a good surface and improve the adhesion between the powders and the substrate [12]. The printing pressure is set to 28 bars for the Al coating, 24 bars for AlSi10Mg, and 20 bars for Scalmalloy. Pressurized and preheated gas is fed into a Laval nozzle, which generates supersonic velocities to accelerate the solid metal particles with a typical size of about 15–45  $\mu\text{m}$ . The particles collide with the substrate in a completely solid state, and then combine with the substrate via the severe plastic deformation caused by the collision to achieve metallic deposition [13]. Finally, a coating with a thickness of  $\sim 2$  mm is obtained after various passes of the deposition for every selected aluminum powder. A detailed schematic view of the CS process is shown in Figure 1a for understanding.

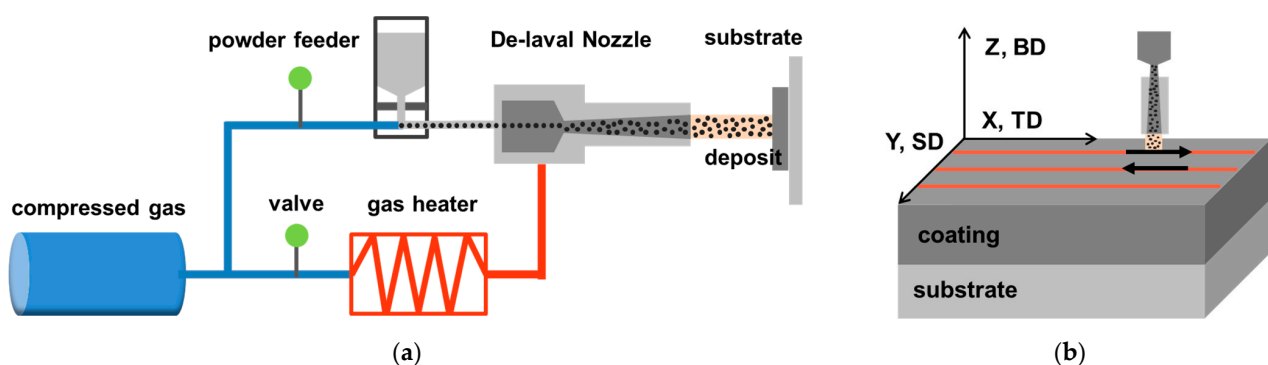


**Figure 1.** Schematic diagram of cold gas dynamic spray: (a) system; and (b) pathway and sampling direction of the coating specimen. The printing directions are indicated.

After the CS process, the coating specimens of three aluminum materials are extracted from the deposits using a grinding wheel to pursue microstructural characterization. SEM equipped with an EBSD detector is used to characterize both the top surfaces and cross sections of the three aluminum materials. The SEM equipment is operated with an acceleration voltage setting at 20 kV with a focused distance of  $\sim 8$  mm. Before EBSD characterization, all the specimens are mounted in a conductive matrix and then polished to a mirror surface finish with a diamond suspension to obtain a surface roughness of approximately 1  $\mu\text{m}$ .

Moreover, the final requirement for the roughness characterized by EBSD is achieved via ion polishing with the voltage at 3 kV for 30 min. An acceleration voltage of 30 kV and a step size of 0.08  $\mu\text{m}$  are used for both SEM and EBSD analysis. SEM analysis is used to investigate the coating microstructures and bonding mechanisms. Meanwhile, the EBSD data is analyzed using the AZtec software from Oxford Instruments, which is aimed to characterize the particles and grains.

### 3. Results and Discussion

A comparative study of CSed aluminum's characteristics is carried out via various microstructural analysis (SEM, EBSD) of the test coating specimens. As the major objective of this study is to investigate the microstructural evolution from the aluminum feedstock powders to the CSed coatings, the characterization of the aluminum feedstock powders is firstly performed. Figure 2a shows the comparative curves of particle size distribution among the three powders. The three powders are irregular and there is a significant difference in size distribution. Figure 2b–d show the morphology of the top surface of three aluminum materials after the deposit process without polishing, representing the typical surface microstructure of the atomized powders.

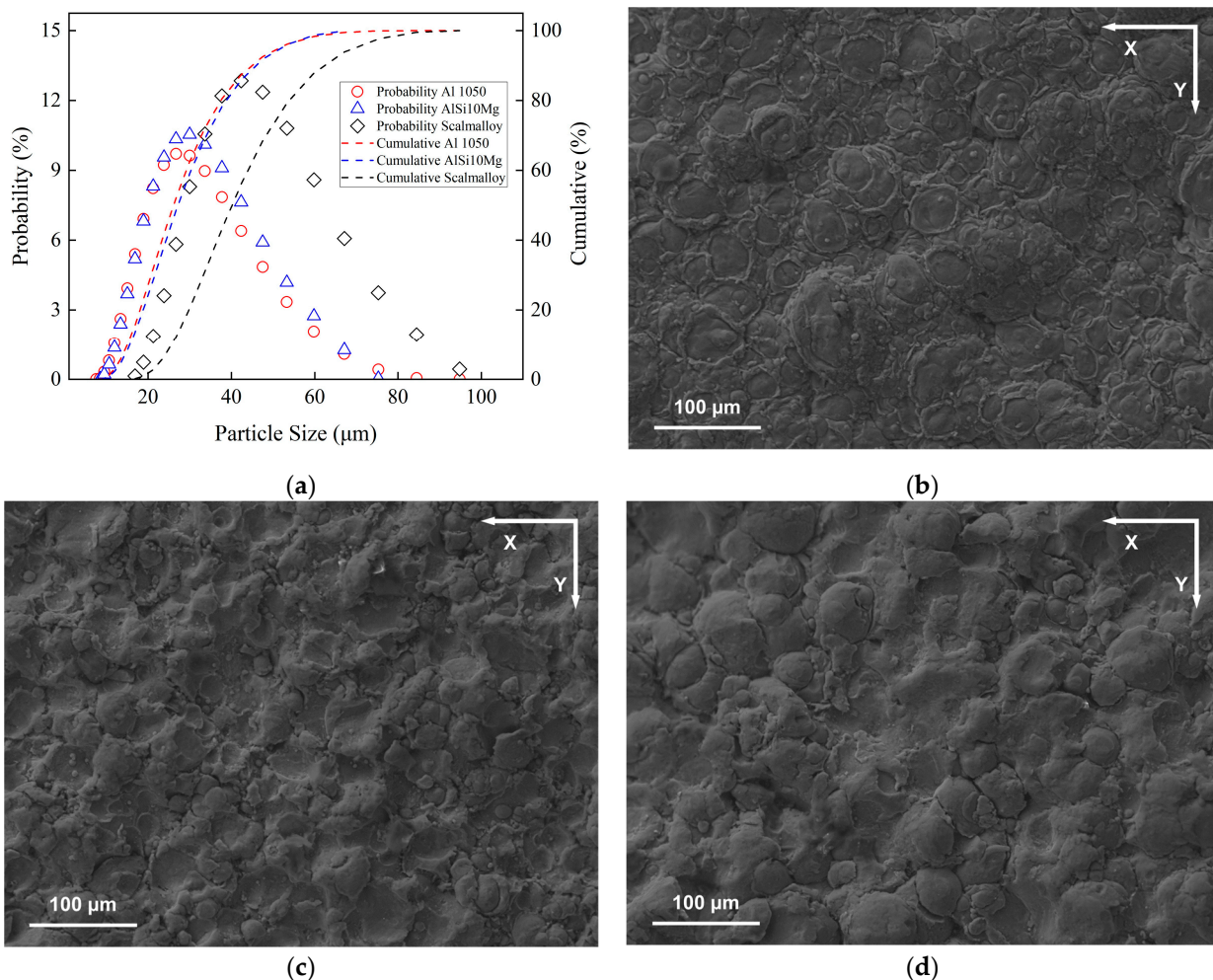


**Figure 2.** (a) Particle size distribution; SEM micrograph showing the top surfaces of the used (b) Al 1050 (c) AlSi10Mg, and (d) Scalmalloy powders fabricated via cold spray coating technology.

The figure captures the typical morphologies of microparticles associated with the said Al 1050, AlSi10Mg, and Scalmalloy feedstock, which maintained an average powder size of 28.680  $\mu\text{m}$ , 28.715  $\mu\text{m}$ , and 42.412  $\mu\text{m}$ , respectively. The three powders are an almost spherical shape. These low magnification images show the general morphology of the top

splats of the aluminum coatings and then provide an overview of the deformed particles. All of the three splats in Figure 2b–d are heavily deformed after impact and the contrast within the aluminum splats are relatively homogeneous. Meanwhile, the high kinetic energy during the high strain rate shearing and the large volume of aluminum particles ensures that the deposited aluminum coatings can be extensively hammered and forged over large areas, resulting in the formation of dense deposits [14]. From the morphology, we can see that there is a good printing quality with only small voids.

Figure 3 shows the grain structure of the Al 1050 coating with two different sections taken from the top surface and near the coating–substrate interface, respectively. Both of the grain micrographs of CSed samples' sections present highly deformed splats as the typical characteristic features of the cold gas dynamic spray process. It is clear that Al 1050 particles experienced significant plastic deformation after bonding and deformation. The grain boundaries, coating boundaries, and inter-particle boundaries became visible in the as-fabricated stage via the EBSD characterization as shown in Figure 3a,b. The boundaries between grains are more pronounced than that at the grain boundaries, implying that the inter-particle grain boundary is the weak position after high-speed deposition [15]. Moreover, it can be seen that the microstructure exhibits obvious anisotropic microstructural features with different sections. During the high strain rate shearing process, aluminum particles undergo a severe deformation with a high velocity, leading to a significant flattening and compression in the deposit direction. In addition, it is interesting to observe that recrystallization occurred not only inside the impact particles, but also across the coating boundaries as well as the grain boundaries [16].

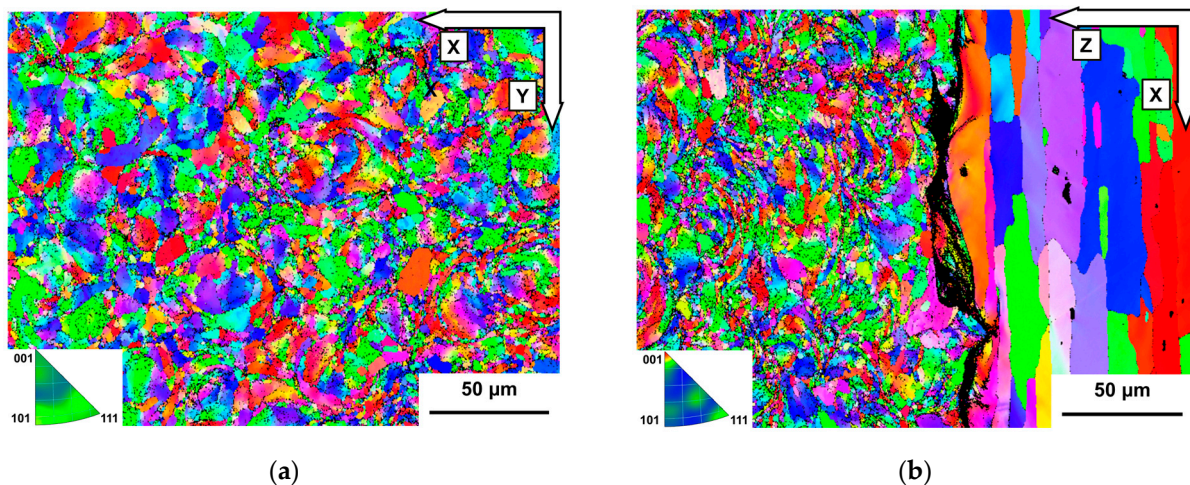


**Figure 3.** IPF map of (a) surface and (b) cross section of Al 1050 coating.

Comparative analyses reveal a similar phenomenon that occurred in the top surface as well as in the cross section of all three aluminum coating materials. Figure 4 shows the EBSD micrographs from the CSed AlSi10Mg coating cross-sections on the top surface and near the coating–substrate interface. Figure 4b with low magnification shows the general morphology of the coating cross-section presenting flattened particles under severe plastic deformation. It presents a specific area with an EBSD scan that contains both sides of the coating and the substrate. The black area shows that the scan algorithm cannot identify both the grain structure and the orientation due to the severe distortion of the lattice. This phenomenon is commonly observed in CSed deposits. The specific characteristic features of the AlSi10Mg particles shown in Figure 4 can also be seen that there are more obvious narrow gaps at most of particle–particle interfaces in the coating. A distinguishing feature of the scan is that only the substrate can be indexed by EBSD, while indexing is almost impossible in the coating. This reflects that the high residual stress and strain present in the CSed coating distorted the phase lattice of AlSi10Mg [17]. At the same time, no indexing is possible from the coating layer into the substrate, which is shown as a long gap between the

coating and the substrate. This indicates the presence of severe deformation in the top layer of the substrate. Figure 5 shows the EBSD micrographs from the CSed Scalmalloy coating cross-section which is taken on the top surface and near the coating–substrate interface. It can be seen that the powder size of Scalmalloy is significantly larger than that of AlSi10Mg. The same thing occurs during the recrystallized grains' formation after the high strain rate impact.

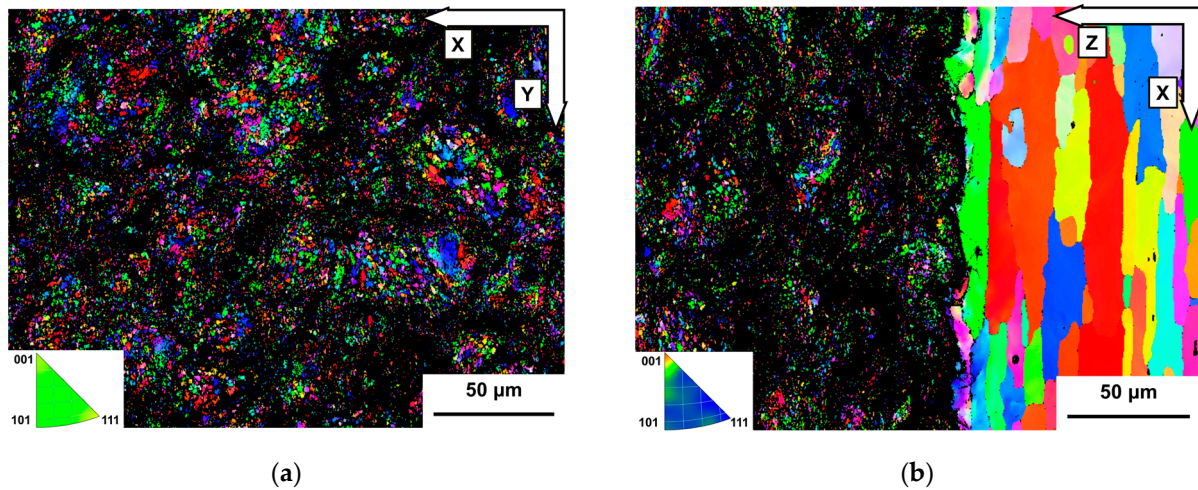


Figure 4. IPF map of (a) surface and (b) cross section of AlSi10Mg coating.

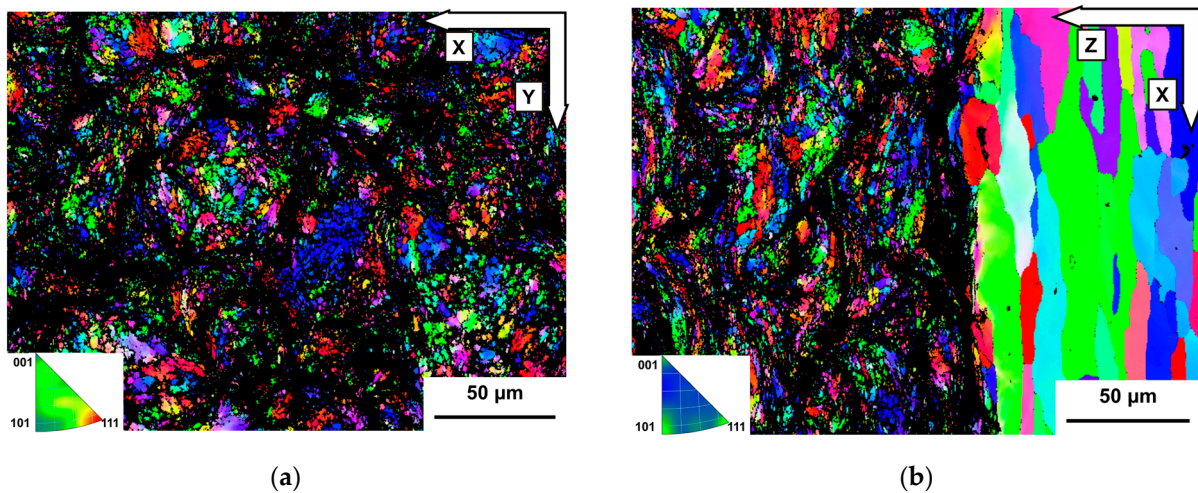
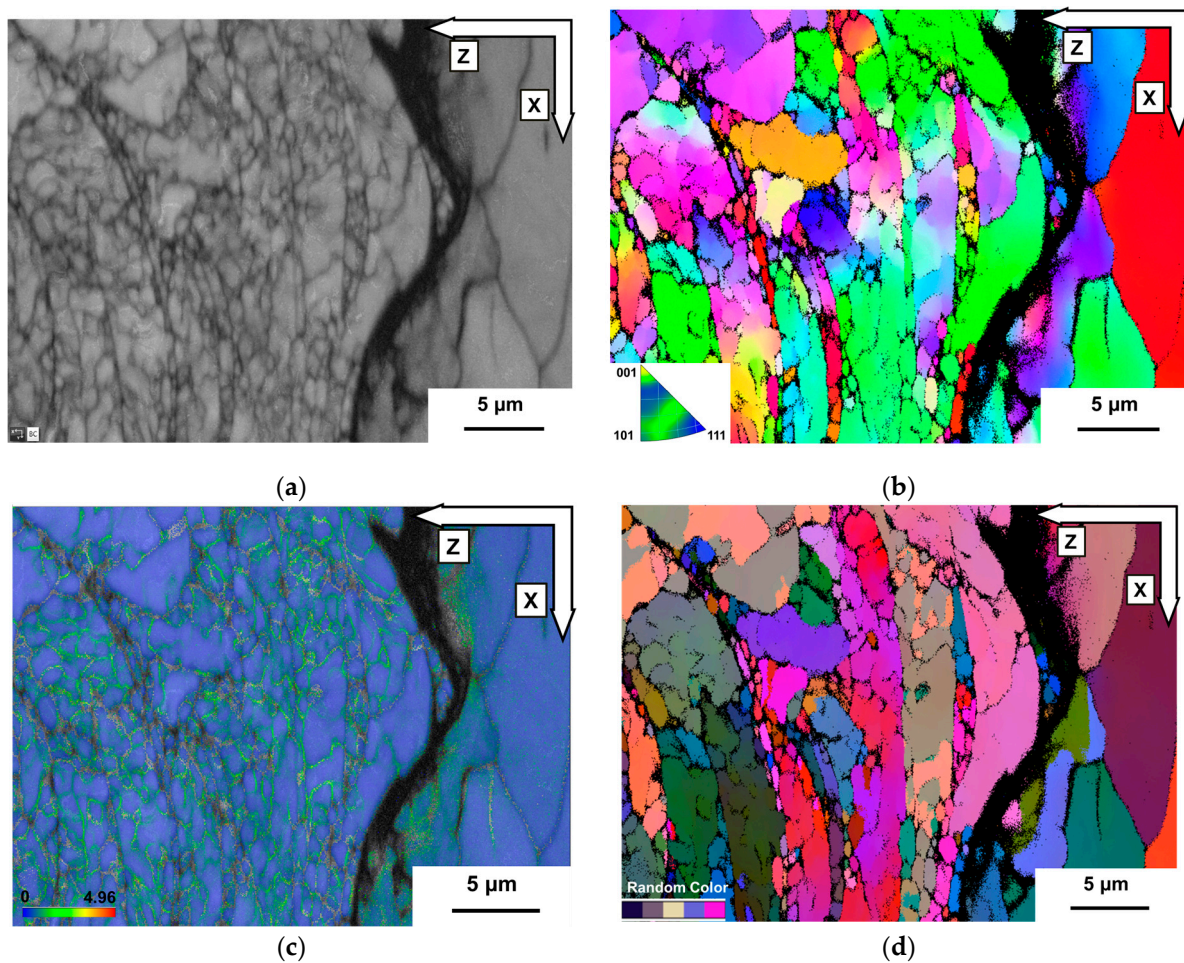


Figure 5. IPF map of (a) surface and (b) cross section of Scalmalloy coating.

Cross sectional view of Al 1050 with high magnification are investigated to further describe the bonding mechanisms and confirm the dynamic recrystallization (DRX) of aluminum particles during the cold spray process. A small scan area with a high scan step size ( $0.02\ \mu\text{m}$ ) is chosen to perform the analysis. Figure 6 shows the EBSD image using the fore scatter detector that can enhance the topological microstructural features of the Al 1050 coating. It shows the cross-sectional EBSD images of the CSed Al 1050 deposit in four different solutions obtained from AZtec. In the as-fabricated state, as shown in Figure 6a, both the inter-particle boundaries and the grain boundaries appear more clearly under high magnification. It can be seen that very fine grains are present in the outer region of the particles. Figure 6b–d show the high-resolution EBSD data obtained from the Al 1050 coating material. Both images reveal that the whole region undergoes severe deformation, especially at the interface of particle–particle and particle–substrate. Moreover, the grains in the center of the particles have less deformation and a larger size. Figure 6b shows the aluminum grains colored using the inverse pole figure. We found

that the aluminum particles had undergone severe plastic deformation under the high strain rate shearing. Figure 6c shows the kernel average misorientation (KAM) map of the aluminum grains that reflects the degree of the accumulated strain. The KAM map also reveals that most of the plastic shear strain accumulates in the outer fine-grained regions. The main reason is that the periphery of the particles is severely deformed, while the middle part remained almost unchanged [18]. Meanwhile, dynamic recrystallization occurs at the interface due to the high-speed collision during the cold spray process. Figure 6d shows the Euler angle map colored with different grain orientations.



**Figure 6.** EBSD analysis of Al 1050 coating. (a) EBSD image map showing the presence of very fine grains in the outer region of the particles; (b) IPF map showing grain orientation; (c) Kernel average misorientation (KAM) map revealing the degree of accumulated strain; and (d) Euler angle map showing different grain orientations.

#### 4. Conclusions

Based on the key finding from the microstructural characterization in the last section, a comprehension for the microstructural evolution of CSed aluminum powders has been discussed. The cold gas dynamic spray process has gained the significant attraction in self-consolidated additive manufacturing. Aluminum is an outstanding metal with improved properties used for manufacturing components for the aerospace industry. In this study, a high-pressure cold gas dynamic spray system with helium gas is used to deposit Al 1050, AlSi10Mg, and ScAlMg coating materials. A systematic microstructural characterization of the CSed aluminum coatings has been performed at the microscopic scale using SEM and EBSD characterization. Based on the microstructural examination of the aluminum coatings, the following findings and conclusions are drawn:

During the cold gas dynamic spray process, the aluminum alloys undergoes a high strain rate plastic deformation due to the impact on the substrate resulting in the severe changes of the morphology. The microstructure in aluminum particles near the particle–substrate interface contains several refined grains due to the high lateral plastic flow within the particle during the high strain rate self-consolidation. A similar situation occurs at the particle–particle interface. The region adjacent to the interface of the impacting particles undergoes a high strain rate deformation, thus forming fine grains at the bottom of the particle. Meanwhile, the morphology of splats, recrystallization degree, and lattice distortion after the high strain rate impact are affected by the powder size and distribution and by the mechanical properties.

## 5. Perspectives

Later, we will employ transmission electron microscopy (TEM) to exam the interface bonding between particles or between the particles and the substrate. Due to the impact of the aluminum particles, a high degree of plastic strain is accumulated in the deposited particles. Since it is not yet feasible to experimentally measure the plastic strain at the particle–substrate interface, we will use finite element models for the bonding mechanism of individual particles to understand the induced strain [19].

**Author Contributions:** Writing—original draft preparation J.Q.; methodology, C.V. and R.N.R.; validation, J.L., R.N.R. and M.R.; writing—review and editing, R.N.R. and M.R. All authors have read and agreed to the published version of the manuscript.

**Funding:** The authors would like to thank the CHINA SCHOLARSHIP COUNCIL for grant number 202106220028.

**Institutional Review Board Statement:** Not applicable.

**Informed Consent Statement:** Informed consent was obtained from all subjects involved in the study.

**Data Availability Statement:** Not applicable.

**Conflicts of Interest:** The authors declare no conflict of interest.

## References

1. Raoelison, R.N.; Verdy, C.; Liao, H. Cold gas dynamic spray additive manufacturing today: Deposit possibilities, technological solutions and viable applications. *Mater. Des.* **2017**, *133*, 266–287. [[CrossRef](#)]
2. Raoelison, R.N.; Koithara, L.L.; Costil, S. Cold spray coating of PEEK surface by copper deposition: Interfacial adhesion at high deposition efficiency and bonding strength. *CIRP J. Manuf. Sci. Technol.* **2021**, *35*, 63–68. [[CrossRef](#)]
3. Raoelison, R.N.; Koithara, L.L.; Costil, S.; Xie, X. Capability of cold spraying to obtain high deposition efficiency for the metallization of PEEK. In Proceedings of the International Thermal Spray, Yokohama, Japan, 26–29 May 2019. [[CrossRef](#)]
4. Koithara, L.L.; Raoelison, R.N.; Costil, S.; Xie, X. High deposition efficiency and delamination issues during high-pressure cold spraying metallization of PEEK using spherical copper powders. *Int. J. Adv. Manuf. Technol.* **2020**, *107*, 4427–4436. [[CrossRef](#)]
5. Raoelison, R.N.; Xie, Y.; Sapanathan, T.; Planche, M.P.; Kromer, R.; Costil, S.; Langlade, C. Cold gas dynamic spray technology: A comprehensive review of processing conditions for various technological developments till to date. *Addit. Manuf.* **2017**, *19*, 134–159. [[CrossRef](#)]
6. Sousa, B.C.; Walde, C.; Champagne, V.K., Jr.; Nardi, A.T.; Sisson Jr, R.D.; Cote, D.L. Rapidly solidified gas-atomized aluminum alloys compared with conventionally cast counterparts: Implications for cold spray materials consolidation. *Coatings* **2020**, *10*, 1035. [[CrossRef](#)]
7. Ren, Y.; Liu, H.; Zhao, L.; Cui, X.; Shen, Y.; Wang, J.; Xiong, T. Study of microstructural and mechanical anisotropy of 7075 Al deposits fabricated by cold spray additive manufacturing. *Mater. Des.* **2021**, *212*, 110271. [[CrossRef](#)]
8. Koithara, L.L.; Raoelison, R.N.; Costil, S.; Planche, M.P. Powder jet variations using Low Pressure Cold Spraying—For an improvement of the spraying yield. In Proceedings of the International Thermal Spray, Yokohama, Japan, 26–29 May 2019. [[CrossRef](#)]
9. Koithara, L.L.; Raoelison, R.N.; Costil, S. Flow phenomenon of micron-sized particles during cold spray additive manufacturing: High-speed optic observation and characterization. *Adv. Powder Technol.* **2020**, *31*, 1060–1079. [[CrossRef](#)]
10. Raoelison, R.N. Analytical description of solid particles kinematics due to a fluid flow and application to the depiction of characteristic kinematics in cold spraying. *Powder Technol.* **2017**, *319*, 191–203. [[CrossRef](#)]

11. Raelison, R.N.; Koithara, L.L.; Costil, S.; Langlade, C. Turbulences of the supersonic gas flow during cold spraying and their negative effects: A DNS CFD analysis coupled with experimental observation and laser impulse high-speed shadowgraphs of the particles in-flight flow. *Int. J. Heat Mass Transf.* **2020**, *147*, 118894. [[CrossRef](#)]
12. Wu, H.; Xie, X.; Liu, M.; Verdy, C.; Zhang, Y.; Liao, H.; Deng, S. Stable layer-building strategy to enhance cold-spray-based additive manufacturing. *Addit. Manuf.* **2020**, *35*, 101356. [[CrossRef](#)]
13. Raelison, R.N.; Aubignat, E.; Planche, M.P.; Costil, S.; Langlade, C.; Liao, H. Low-pressure cold spraying under 6bar pressure deposition: Exploration of high deposition efficiency solutions using a mathematical modelling. *Surf. Coat. Technol.* **2016**, *302*, 47–55. [[CrossRef](#)]
14. Luo, X.T.; Yao, M.L.; Ma, N.; Takahashi, M.; Li, C.J. Deposition behavior, microstructure and mechanical properties of an in-situ micro-forging assisted cold spray enabled additively manufactured Inconel 718 alloy. *Mater. Des.* **2018**, *155*, 384–395. [[CrossRef](#)]
15. Vaßen, R.; Fiebig, J.; Kalfhaus, T.; Gibmeier, J.; Kostka, A.; Schrüfer, S. Correlation of microstructure and properties of cold gas sprayed Inconel 718 coatings. *J. Therm. Spray Technol.* **2020**, *29*, 1455–1465. [[CrossRef](#)]
16. Chen, C.; Xie, Y.; Liu, L.; Zhao, R.; Jin, X.; Li, S.; Huang, R.; Wang, J.; Liao, H.; Ren, Z. Cold spray additive manufacturing of Invar 36 alloy: Microstructure, thermal expansion and mechanical properties. *J. Mater. Sci. Technol.* **2021**, *72*, 39–51. [[CrossRef](#)]
17. Lek, J.Y.; Bhowmik, A.; Tan, A.W.; Sun, W.; Song, X.; Zhai, W.; Buenconsejo, P.J.; Li, F.; Liu, E.; Lam, Y.M.; et al. Understanding the microstructural evolution of cold sprayed Ti-6Al-4V coatings on Ti-6Al-4V substrates. *Appl. Surf. Sci.* **2018**, *459*, 492–504. [[CrossRef](#)]
18. Feng, S.; Guan, S.; Story, W.A.; Ren, J.; Zhang, S.; Te, A.; Gleason, M.A.; Heelan, J.; Walde, C.; Birt, A.; et al. Cold spray additive manufacturing of CoCrFeNiMn high-entropy alloy: Process development, microstructure, and mechanical properties. *J. Therm. Spray Technol.* **2022**, *31*, 1222–1231. [[CrossRef](#)]
19. Adaan-Nyiak, M.A.; Tihamiyu, A.A. Recent advances on bonding mechanism in cold spray process: A review of single-particle impact methods. *J. Mater. Res.* **2023**, *38*, 69–95. [[CrossRef](#)] [[PubMed](#)]

**Disclaimer/Publisher’s Note:** The statements, opinions and data contained in all publications are solely those of the individual author(s) and contributor(s) and not of MDPI and/or the editor(s). MDPI and/or the editor(s) disclaim responsibility for any injury to people or property resulting from any ideas, methods, instructions or products referred to in the content.